Supporting Information

Single-Molecule Observation of Photocatalytic Reaction in TiO_2 Nanotube: Importance of Molecular Transport through Porous Structures

*Kazuya Naito, Takashi Tachikawa, Mamoru Fujitsuka, and Tetsuro Majima**

The Institute of Scientific and Industrial Research (SANKEN), Osaka University, Mihogaoka 8-1, Ibaraki, Osaka 567-0047, Japan

Contents

S1. Movies of the Single-Molecule Observations of the Photocatalytic Reactions in the Macropores (Movie S1) and Mesopores (Movie S2) of a Single TiO_2 Nanotube

These movies show the single-molecule observations during the photocatalytic reactions that occurred in a single TiO_2 nanotube. To initiate the photocatalytic reaction, the TiO_2 nanotube on the cover glass was totally irradiated by UV light (365 nm). The UV light intensity is weakened using the neutral density filter (Olympus, 32ND12 (12% transmission)) to prevent the auto-oxidation of the aminophenyl fluorescein (APF) caused by the intense UV irradiation (see also Figure S6). During the UV irradiation, the photocatalytic reaction can be observed by the generation of the emissive fluorescein in the reaction between the APF and $^{\bullet}OH$ molecule formed by the photocatalytic reaction (see Figure 1 in the main text). Movies S1 and S2 show the macropores and mesopores shown in Figures 3A and 3B, respectively. The movies are in real time. In Movie S1, the fluorescein molecule is observed as a fluorescence burst, which can be seen only within the time resolution (33 ms), due to the fast diffusion in the macropore. In contrast, in Movie S2, the fluorescein molecule generated by the photocatalytic reaction can be easily observed on the nanotube as the fluorescent spot slightly diffused. These observations directly indicate the facile diffusion in the pores. Based on these movies, the apparent quantum yield of the generation of $^{\bullet}OH$ in the TiO_2 nanotube (counting of the fluorescence spots) can be estimated.

S2. Generation Mechanism of $^{\bullet}OH$ during the TiO_2 Photocatalytic Reaction

Historically, $^{\bullet}OH$ has been considered to be generated by the oxidation of water (H_2O) in the photogenerated hole (h^+) on the surface of TiO_2 after UV irradiation as follows:[1]

$$TiO_2 + h\nu \rightarrow e^- + h^+, \quad (1)$$

$$H_2O + h^+ \rightarrow {}^\bullet OH + H^+. \quad (2)$$

However, Nakamura et al. have clearly revealed that the oxidation of H_2O is initiated by the nucleophilic attack of a H_2O molecule on h^+ at a surface lattice O site, not by oxidation of the surface OH group by h^+.[2] Therefore, the oxidation of H_2O by h^+ is no longer the generation mechanism of $^\bullet OH$. Recently, Tatsuma et al. proposed that the $^\bullet OH$ generated by the photodecomposition of H_2O_2 plays an important role in the photocatalytic oxidation, even away from the TiO_2 surface.[3] In this case, H_2O_2 is formed by the disproportionation of $O_2^{\bullet-}$, which is generated by the reaction between O_2 with electrons (e^-) in TiO_2 as follows:

$$O_2 + e^- \rightarrow O_2^{\bullet-}, \quad (3)$$

$$O_2^{\bullet-} + H^+ \rightarrow HO_2^\bullet, \quad (4)$$

$$2HO_2^\bullet \rightarrow H_2O_2 + O_2, \quad (5)$$

$$H_2O_2 + h\nu \rightarrow 2{}^\bullet OH. \quad (6)$$

In addition, Nosaka et al. have investigated the generation mechanism of $^\bullet OH$ by observation of the laser-induced fluorescence (LIF) intensity arising from the $^\bullet OH$ that diffused after the excitation of TiO_2.[4,5] During the excitation at 266 and 355 nm, they observed that the differences in the $^\bullet OH$-LIF intensities were within a factor of 2 at most, in spite of the differences in the absorption coefficients of H_2O_2 between 266 and 355 nm ($\sigma(265\text{ nm}) = 4.4\times10^{-20}$ cm^2, $\sigma(355\text{ nm}) < 5.3\times10^{-22}$ cm^2).[5] Accordingly, they claimed that the plausible reaction mechanism of the generation of $^\bullet OH$ is the reduction of H_2O_2, not the photodecomposition as follows:

$$H_2O_2 + e^- \rightarrow {}^{\bullet}OH + OH^-. \quad (7)$$

Until now, the generation mechanism of $^{\bullet}OH$ had not been determined and is still a controversial issue. In either case, there is no doubt that $^{\bullet}OH$ can be generated during the TiO_2 photocatalytic reaction in the aqueous phase and gas phase.[3-8] In our experiment, $^{\bullet}OH$ is used for the indicator of the photocatalytic activity and detected by the specific fluorescent probe, APF, at the single-molecule level.

S3. Experimental Procedures

Materials. For the sol-gel template syntheses of the TiO_2 and SiO_2 nanotubes, commercial porous alumina membranes, in which the diameter of the nanochannels is ca. 200 nm, were purchased from Whatman (Anodisk 47). TiF_4 was purchased from Aldrich and used as the precursor of the TiO_2 nanotubes. $SiCl_4$, CCl_4, methanol, ethanol, and ammonia solution (28%) were purchased from Wako, and 3'-(*p*-aminophenyl) fluorescein (APF) was purchased from Daiichi Pure Chemicals Co., Ltd. Sodium dihydrogenphosphate anhydrate (NaH_2PO_4), and disodium hydrogenphosphate (Na_2HPO_4) for the preparation of the phosphate buffer, and HCl, NaOH and dimethylsulfoxide (DMSO) were purchased from Nacalai Tesque, Inc. All the reagents were used as supplied.

The cover glasses and slide glasses were purchased from Matsunami Glass and cleaned by sonication in a 20% detergent solution (As One, Cleanace) for 6 h, followed by repeated washings with warm running water for 30 min. Finally, the cover glasses were washed again with Milli-Q water.

Epoxy glue (High-speed Epo., Konishi Co., Ltd., Japan) and double-sided tape (Nice Tack, Nichiban Co., Ltd., Japan) were used for the preparation of the flow chamber in the single-molecule experiment.

Synthesis of TiO_2 and SiO_2 Nanotubes. TiO_2 nanotubes were synthesized according to the procedures reported by Imai et al.[9] The TiF_4 solution (0.04 M, pH 2.0) was prepared by dissolving TiF_4 into Milli-Q water and the pH was adjusted by the addition of HCl or an ammonia solution. The alumina porous membranes (Anodisk 47) were immersed in the TiF_4 solution and maintained at 60 °C for 10 h. After the thermal treatment, the membranes were removed from the TiF_4 solution. TiO_2 nanoparticles formed by the hydrolysis of TiF_4 were deposited not only on the walls of the nanochannels, but also on the surfaces of the membranes. The TiO_2 thin film on both surfaces of the membranes were removed by polishing with sandpaper (1500 grid) prior to the immersion in a 6 M NaOH solution used for dissolving the alumina template, so that the liberated TiO_2 nanotubes rather than that of the bundles can be obtained. After dissolving of the template, the liberated TiO_2 nanotubes dispersed in an alkaline solution were filtered and then repeatedly washed with deionized water. The resulting TiO_2 nanotube powder was calcined at 400 ºC for 6 h to enhance the crystallinity and thus, the photocatalytic activity. TEM images and XRD pattern of the TiO_2 nanotube after the calcination are shown in Figure S1 and S2, respectively. These images clearly show the tubular structure of the TiO_2 nanotubes (the diameter is ca. 150 nm), which have a wall of nanocrystals, and confirmed the formation of the anatase phase.

SiO_2 nanotubes were synthesized according to the procedures reported by Kovtyukhova et al.[10] and used for the control experiment shown in Figure 3E in the main text. (1) An alumina porous membrane was immersed in a 67 mol% $SiCl_4$ solution of CCl_4 for 2 min, then quickly washed with CCl_4 to remove any unreacted $SiCl_4$ from the surfaces. (2) The membrane was then soaked in CCl_4 for 15 min to remove away unbound $SiCl_4$ from the pores. (3) Finally, the membrane was washed with CCl_4/MeOH (1:1 volume) (2

min) and ethanol (5 min) to displace the CCl_4, and dried in ambient air. (4) The membrane was then immersed in deionized water for 5 min, washed with methanol (2 min), and dried in ambient air. These processes (1)-(4) were repeated for 10 cycles. The number of cycles directly corresponds to the wall thickness of the SiO_2 nanotube. After polishing the SiO_2 thin film on both surfaces with sandpaper, the membrane containing the SiO_2 nanotubes was immersed in 50% H_2SO_4, to liberate the SiO_2 nanotubes from the membrane. The dispersion of the SiO_2 nanotubes in an acid solution was filtered and then repeatedly washed with Milli-Q water. TEM images of the SiO_2 nanotube are shown in Figure S1. This image clearly indicates a relatively thick wall (ca. 30 nm), a diameter of 170 nm, and a smooth surface on the wall compared to that of the TiO_2 nanotubes. Thus, the SiO_2 nanotube does not contain mesopores.

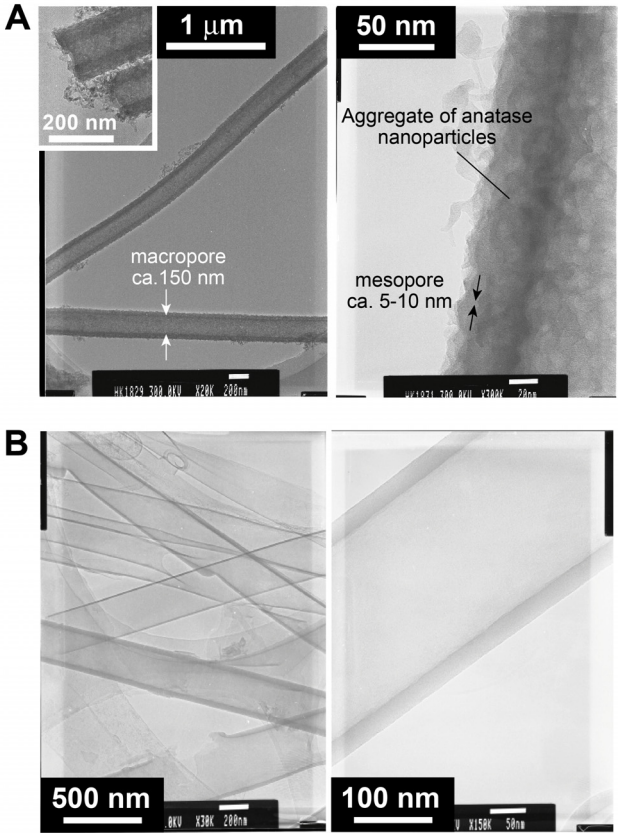

Figure S1. TEM images of the TiO_2 (A) and SiO_2 nanotubes (B) synthesized by the sol-gel template method. The diameter of the synthesized nanotubes is directly related to the alumina porous membrane used as the template (Whatman, Anodisk 47, pore diameter ca. 200 nm). The porous structures of the TiO_2 nanotube, i.e., a straight macropore and mesopores between the anatase particles, are visualized. In the case of the SiO_2 nanotube, which has a smooth surface on the nanotube compared with that of the TiO_2 nanotube, only a straght macropore can be observed.

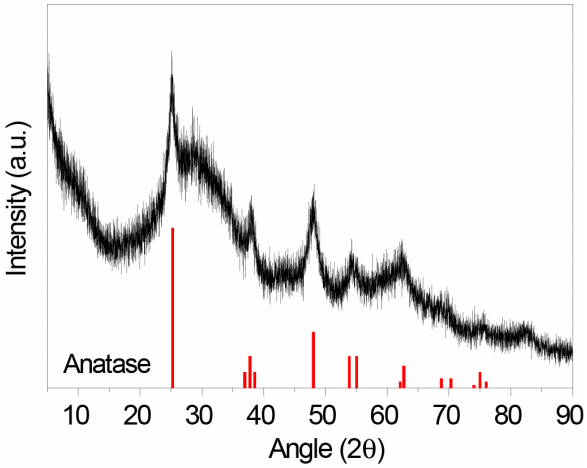

Figure S2. XRD pattern of TiO_2 nanotube synthesized by the sol-gel template method using the hydrolysis of TiF_4 after calcination at 400 ºC for 6 h. The data were measured using the TiO_2 nanotube powder immobilized on the glass. The hollow pattern is from the glass as the substrate. The red bars represent the standard diffraction data for anatase (JCPDS, No. 21-1272).

Sample Preparation. The experiment on a single TiO_2 nanotube is conducted by using a custom-made sample chamber; in this chamber, the same nanotube can be observed under different substrate solutions. The sample is composed of the nanotube-immobilized cover glass and the slide glass possessing two holes (inlet and outlet) through while the substrate solution flowed (Figure S3). Prior to the preparation of the sample, the slide glass was drilled out using a diamond drill to create the two holes as the inlet and outlet. The nanotube-immobilized cover glass was prepared by spin-coating the TiO_2 or SiO_2 nanotube solution on a clean cover glass at 1000 rpm for 15 s, followed by annealing the nanotube-coated cover glass at 100 °C for 1 h in order the nanotubes on the cover glass not to peel off upon the flowing of the substrate solution. After the annealing, the nanotube-immobilized cover glass was repeatedly washed with Milli-Q water and dried in an inert gas. The cover glass was placed on the drilled slide glass with a double-sided adhesive spacer. The edges of the cover glass were sealed using epoxy glue so as not to allow the solution to leak from the chamber.

In the TiO_2 nanotube experiments, the phosphate buffer solution (pH 7.4, 0.1 M) of APF (500 nM), or the mixture of APF (500 nM) and DMSO (100 mM), was used as the substrate solution. In the control SiO_2 nanotube experiment, the phosphate buffer solution (pH 7.4, 0.1 M) of APF (500 nM) was used (see also Figure S6).

The solution was loaded into the chamber from the inlet hole using a pipette tip. The solution in the chamber was exchanged with the other solutions of different concentrations during the single-nanotube measurements.

Ensemble Spectroscopy. The steady-state UV-Vis absorption and fluorescence spectra were measured using a Shimadzu UV-3100 and a Hitachi 850, respectively.

Single-Molecule Fluorescence Measurements at the Single-Nanotube Level. The experimental setup is based on an Olympus IX71 inverted fluorescence microscope. A schematic illustration for the experimental setup is shown in Figure S3. All the experimental data were obtained at room temperature. The position of the TiO_2 or SiO_2 nanotube is determined by the transmission image obtained from the illumination using the halogen lamp (Olympus, U-LH100L-3) above the sample. Light emitted from a CW Ar ion laser (488 nm, 50 mW; Melles Griot, IMA101010BOS) was reflected by the first dichroic mirror (Olympus, RDM450), which reflects wavelengths longer than 450 nm and is transparent to the light shorter than 450 nm, toward a second dicroic mirror (Olympus, DM505). The CW laser light passing through an objective lens (Olympus, UPlanSApo, 1.40 NA, 100×) after the reflection at a second dichroic mirror was totally reflected at the cover glass-water interface that generated an evanescent field (the penetration depth d from the interface is ca. 200 nm), which enables one to detect a single fluorescent

probe in a single nanotube. For excitation of the TiO_2 nanotube, light emitted from a mercury lamp (0.2 mW cm^{-2}, Ushio, USH-102D) passing through a band-pass (BP) filter (Olympus, BP330-385) was passed through an object lens. The switching of the BP filters for the UV excitation was automatically manipulated by the shutter controller (Sigma Koki, SSH-C4B).

For imaging, the fluorescence emission from the single fluorescein molecules generated in the nanotube on the cover glass was collected using an oil-immersion microscope objective, magnified by a 1.6× built-in magnification changer (thus, net magnification is 160×), and passed through the emission filters to remove the undesired scattered light (Olympus, BA510-550 and SCF500), and then imaged by an electron-multiplying charge-coupled device (EM-CCD) camera (Roper Scientific, Cascade II:512). The images were processed using Image-Pro Plus software (Roper Scientific, ver. 6.2), ImageJ software (http://rsb.info.nih.gov/ij/), or custom-made software (Library, Gray Val32). The images were recorded at the frame rate of 30 frames s^{-1}. The 16-bit experimental data were converted to 8-bit data for the analysis.

For spectroscopy, only the fluorescence that passed through a slit entered the imaging spectrograph (Acton Research, SP-2356) equipped with an EMCCD camera (Princeton Instruments, PhotonMAX:512B). The width of the slit was 200 μm, which corresponded to 1.25 μm at the specimen, because the images at the slit were magnified by 160×. The spectra were typically integrated for 5 s. The fluorescence spectra of fluorescein were cut by a long-pass filter (Olympus, BA510IF) on the blue edge. The spectrum detected by the EMCCD camera was stored and analyzed using a personal computer. The fluorescence spectra of fluorescein in solution (1 μM) and at the single-molecule level obtained under the microscope are shown in Figure S4.

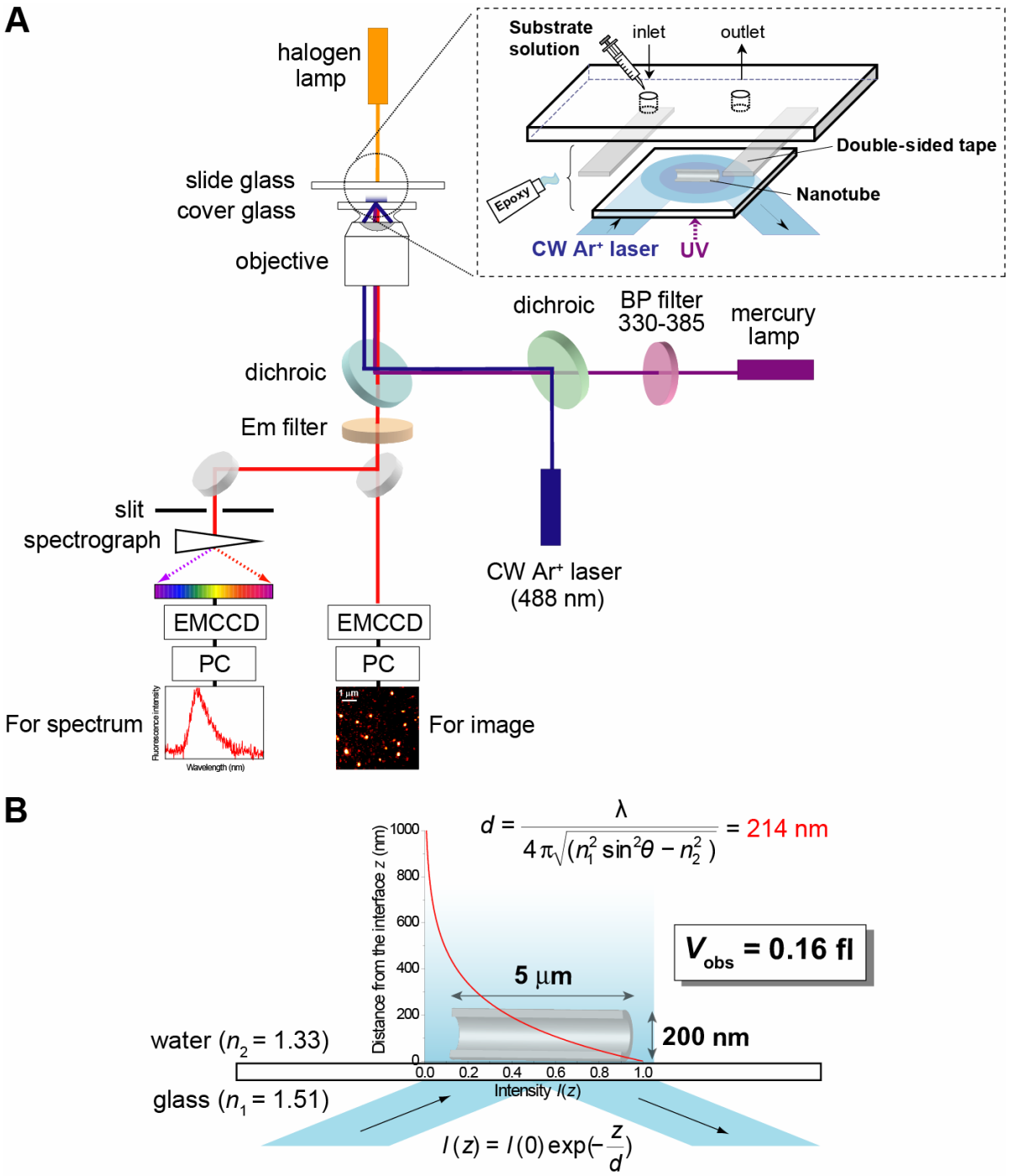

Figure S3. (A) Experimental setup for imaging of photocatalytic reaction occurring on a single nanotube using the flow chamber, which is composed of a drilled slide glass and the nanotube-immobilized cover glass with a double-sided adhesive spacer. (B) Configuration of the single-molecule fluorescence detection in a single-nanotube using total internal reflection fluorescence microscopy (TIRFM). The value of the penetration depth *d* of an evanescent wave from the interface (214 nm) is a very good match with the diameter of the nanotube (ca. 200 nm), indicating that all the fluorescent molecules in the nanotube can be efficiently excited without detecting the fluorescence coming from the molecules above the nanotube. The volume (V_{obs}) of the typical nanotube (diameter 200 nm, length 5 μm) is 0.16 fl, corresponding to the observed volume from the confocal fluorescence microscopy (0.1-1 fl). Since the fluorescent molecule diffusing in the single-nanotube can be efficiently excited, the single-molecule fluorescence detection is possible even when freely diffusing in the water-filled nanotube.

S4. Possible Detection of Fluorescein in the Nanotube

Prior to the experiment on a single nanotube, it was required to precisely consider whether or not the fluorescence of a single fluorescein molecule generated in the nanotube can be detected. In a typical single-molecule fluorescence measurement, the fluorescent molecule being observed must be immobilized on the surface by other methods, such as chemical modification using a reactive functional group, the tethering by a site-specific tag (e.g., the biotin-streptavidin linkage) and the encapsulation in a pore of a gel matrix, enabling one to characterize the temporal behavior of a single molecule of interest over an extended time.[11] In this study, however, the fluorescein molecules formed by the photocatalytic reaction (TiO_2 nanotube) or the auto-oxidation of APF by the intense UV irradiation (SiO_2 nanotube) must freely diffuse in the water-filled nanotube and not be immobilized on the surface, by considering the fact that the size of the fluorescein molecule (ca. 1 nm) is much smaller than the diameter of the nanotubes (ca. 150 nm). In addition, the fluorescein molecule cannot be adsorbed on the surface of the nanotubes due to the electronic repulsion, based on the fact that both the fluorescein molecule (the values of pK_a for the monoanion and dianion are 4.31 and 6.43, respectively)[12] and the nanotubes (the isoelectric points of TiO_2 and SiO_2 are 2.7-6.0 and 2.0-5.0, respectively)[13,14] are negatively charged under this experimental condition (pH 7.4).[15] Furthermore, if the fluorescein molecule adsorbs on the TiO_2 nanotube, the fluorescence signals from fluorescein molecule cannot be observed due to the fluorescence quenching on the surface of the TiO_2 nanoparticle in the nanotube, by taking into account the free energy change for the electron injection (–0.57 eV) calculated from the energy levels of the singlet excited state of fluorescein (–1.13 V vs NHE, estimated from the oxidation potential of the fluorescein dianion (+1.34 V vs NHE)[16]

and the energy for the excitation to the S_1 state (2.47 eV) determined from average wavenumbers of the first absorption and emission maxima) and the conduction band of TiO_2 in water at pH 7.4 (–0.57 V vs NHE).[17]

To detect a single fluorescent molecule freely diffusing in solution, the observed volume must be reduced to 0.1-1 fl,[18] a volume that corresponds to the signal-to-noise (S/N) ratios of 10^3-10^2, based on the background noise of Raman scattering from water as a solvent.[19] The availability for use with the confocal fluorescence microscopy is based on this consideration.[19]

Considering the average diameter (ca. 200 nm) and the length (ca. 5 μm) of the nanotubes, the nanotube volume was calculated to be 0.16 fl. Additionally, the penetration depth *d*, which determines the illuminated region from the cover glass-water interface, is given by,[11]

$$d = \frac{\lambda}{4\pi\sqrt{(n_1^2 \sin^2\theta - n_2^2)}},$$

where θ is the angle of incidence, λ is the wavelength of light (488 nm) and n_1 and n_2 are the refractive indices of the cover glass (1.51) and water (1.33), respectively. This equation allows us to determine the penetration depth for the experiment on a single nanotube to be 214 nm (In this case, the depth was calculated for 1º above the critical angle ($\theta_c = \sin^{-1}(n_2/n_1) = 61.7º$)). This value is in very good agreement with the diameter of the nanotube (200 nm), indicating that all the fluorescein molecules in the nanotube can be efficiently excited without detecting the fluorescence due to the molecules above the nanotube. This experimental condition is described in Figure S3B.

Therefore, these experimental conditions fully satisfy the single-molecule fluorescence detection of the fluorescein molecule in a nanotube even when freely diffusing. Namely, the experiment on a single

nanotube is analogously utilized for the confocal fluorescence microscopy. Under this condition, the fluorescence of fluorescein is observed as a fluorescence burst, which can be observed only within the time resolution of the measurement (33 ms), since the average diffusion length of fluorescein for the time resolution is estimated to be 4.3 μm,[20] that is comparable to the average length of the nanotube (5 μm). In fact, the fluorescein can diffuse out of the nanotube faster than 33 ms because both ends of the nanotube are not plugged. The residence time (t_R) of fluorescein can be calculated from the line profile of fluorescence, as shown in the next section.

Figure S4 shows the fluorescence spectra of the fluorescence spot emerged in the mesopore (red), of which diffusion is slow enough to detect the fluorescence spectra. The spectral peak is consistent with that obtained using the 1 μM fluorescein solution measured under the microscope (blue). The green line shows the fluorescence spectra of the 1 μM fluorescein solution measured by a conventional fluorometer (Hitachi 850). The apparent red shift of the spectra obtained under the microscope is due to the use of a long pass filter (Olympus, BA510IF), which cut the light below 510 nm. This result clearly shows the generation of fluorescein induced by the TiO_2 photocatalytic reaction.

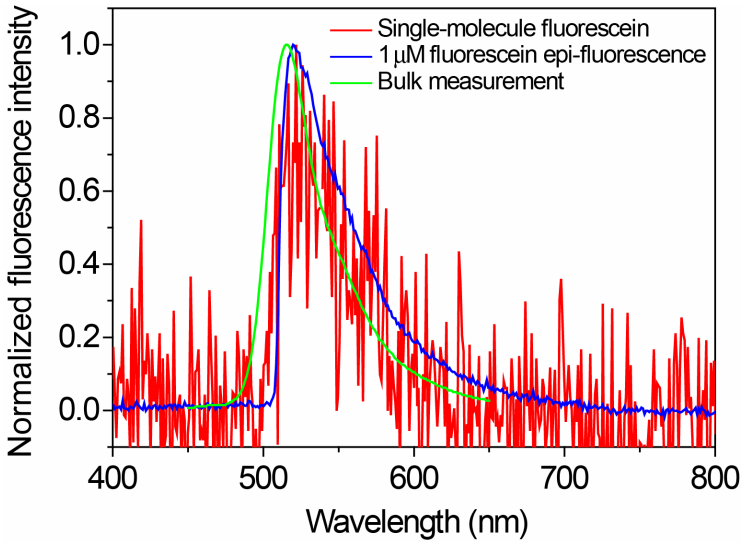

Figure S4. Fluorescence spectra of the single-molecule fluorescent spot generated in the mesopore of the TiO_2 nanotube during the TiO_2 photocatalytic reaction (red). The fluorescence spectra of the 1 μM fluorescein in phosphate buffer solution (pH 7.4) under the epi-fluorescence illumination is shown for comparison (blue). The green line shows the fluorescence spectra of the 1 μM fluorescein solution measured by a conventional fluorometer (Hitachi 850). The apparent red shift of the peak wavelength of the spectral data obtained under the microscope (red and blue) compared to the bulk measurement (green) is due to the use of a long-pass filter (BA510IF), which cut the light below 510 nm.

S5. Estimation of the Residence Time in the TiO_2 Nanotube

The residence time in the nanotube, t_R, can be calculated from the equation of Brownian motion in one dimension, $\langle r^2 \rangle = 2Dt_R$, where $\langle r^2 \rangle$ is the mean-square displacement defined by the square of the half the width of the Gaussian distribution (σ, ca. 500 nm), and D is the diffusion coefficient of fluorescein in solution (2.8×10^{-10} m^2 s^{-1}).[20b] As a result, the average t_R is estimated to be 4.5×10^{-4} s (450 μs).

S6. Estimation of the Apparent Quantum Efficiency of the •OH Generation

We investigated the apparent quantum efficiency of the generation of •OH defined as the ratio of the number of generated fluorescein molecules (N_{Fl}) to the number of the photons irradiated on the TiO_2 nanotube (N_{TiO2}), as described by the following equation,

$$\text{The apparent quantum efficiency of the generation of } {}^{\bullet}\text{OH} = \frac{\text{The number of generated fluorescein molecules } (N_{Fl})}{\text{The number of photons irradiated to } TiO_2 \text{ nanotube } (N_{TiO2})}.$$

In the experiment on a single nanotube, N_{Fl} is estimated by counting the number of fluorescence spots having the fluorescence intensity above the threshold in the histograms (see Figure 2C in the main text). N_{TiO2} can be estimated by the power of the UV lamp using the neutral density filter (2.4×10^{-5} W cm^{-2}), the area of the TiO_2 nanotube irradiated with UV (diameter (200 nm) × contour length (l μm)), the irradiation time for the counting of fluorescein, and the photon energy at 365 nm (5.4×10^{-19} J).

In the bulk experiment, 2 ml of 500 nM APF phosphate buffer solution (pH 7.4) with dispersed TiO_2 nanotubes (0.5 mg ml^{-1}) in a 1 cm × 1 cm quartz cell was irradiated by a UV lamp. Therefore, N_{TiO2} can be estimated by the power of the UV lamp (irradiation intensity, 15 mW), the irradiation time, and the photon energy at 365 nm (5.4×10^{-19} J).

As shown in Figure S5A, after UV irradiation, the peaked fluorescence intensity at 514 nm gradually increased, indicating the generation of fluorescein induced by the photocatalytic reaction. For the estimation of the number of fluorescein molecules, the differential fluorescence intensity is shown. The inset in Figure S5A shows the time course of the fluorescence intensity in a 500 nM APF phosphate buffer solution during the UV irradiation. Despite the absence of the TiO_2 nanotubes, the fluorescence slightly increased due to the auto-oxidation of APF by the direct UV irradiation, which is commonly an unavoidable phenomenon (as discussed in the next section). N_{Fl} can be estimated from the differential fluorescence intensity using the calibration curve, which was obtained by measuring the fluorescence intensity of the fluorescein phosphate buffer solution with dispersed TiO_2 nanotubes (0.5 mg ml^{-1}) with varying concentrations to take into account the light scattering of the solution.

Figure S5B is a plot of the relationship between N_{Fl} and N_{TiO2} in the photocatalytic reaction (open circle) and the auto-oxidation of APF (solid circle). The apparent quantum efficiency was estimated to be 1.1×10^{-8} by subtracting the slope of the solid circles from that of the open circles.

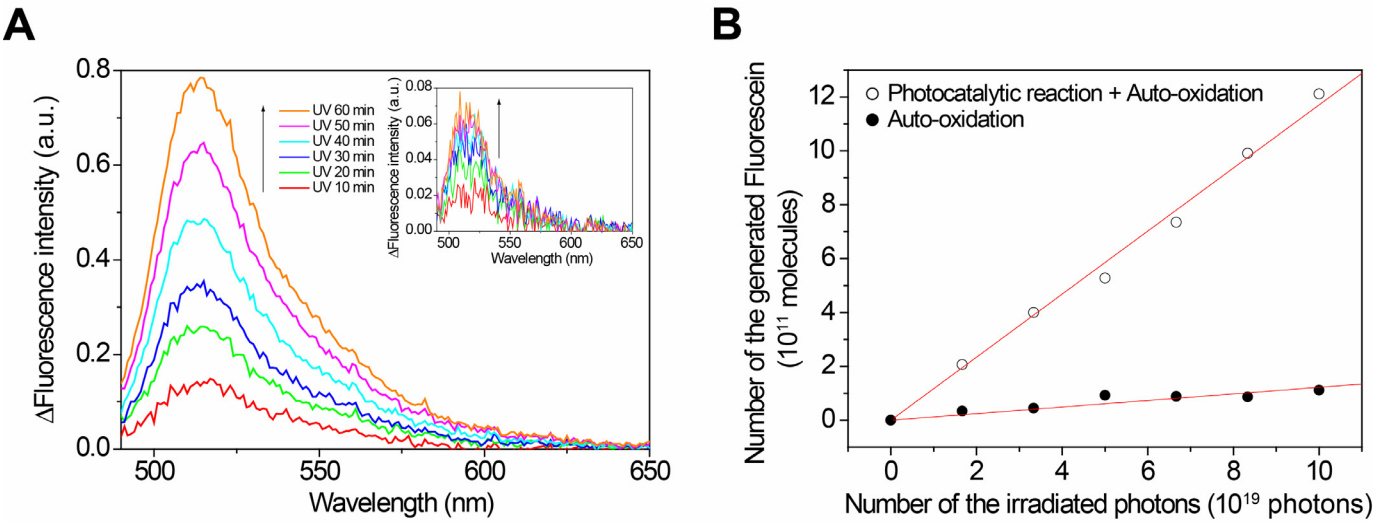

Figure S5. (A) Differential fluorescence intensity of 500 nM APF phosphate buffer solution (pH 7.4) with dispersed TiO_2 nanotubes (0.5 mg ml^{-1}) after 365-nm UV irradiation. Inset shows the differential fluorescence intensity of 500 nM APF phosphate buffer solution (pH 7.4) during the UV irradiation. A slight increase in the fluorescence intensity is due to the auto-oxidation by the direct UV irradiation. (B) The relationship between the number of generated fluorescein molecules and the number of the irradiated photons. The apparent quantum efficiency was estimated to be 1.1×10^{-8} by subtracting the slope of the solid circles from that of the open circles.

S7. Auto-Oxidation of APF Caused by the Intense UV Irradation

As shown in Figure S6A, APF becomes fluorescein not only from the reaction with $^{\bullet}OH$, but also from the auto-oxidation caused by the intense light irradiation. The presence of a slight absorption at 365 nm is responsible for the auto-oxidation. To clarify the effect of the UV irradiation on this phenomenon, the dependence of the UV irradiation power was investigated. For exclusion of the effect by the TiO_2 photocatalytic reaction, the SiO_2 nanotube was used in the experiment. The SiO_2 nanotube immersed in the phosphate buffer solution of 500 nM APF (pH 7.4) is irradiated at different UV light powers. The intensity of the UV light is weakened using the neutral density filter (Olympus, 32ND50 (50% transmission),

32ND25 (25% transmission), and 32ND12 (12% transmission)). Single-molecule events for the generation of the fluorescein molecule by the auto-oxidation are shown in Figure S6B. By increasing the UV irradiation power, the frequency of the auto-oxidation of APF gradually increases. In contrast, the auto-oxidation of APF is significantly suppressed during the weak UV irradiation. For the experiment with the TiO_2 nanotubes, the 32ND12 filter (12% transmission) was used for the complete suppression of the auto-oxidation.

It is worth noting that the single-molecule event in the SiO_2 nanotubes is observed as a fluorescence burst, indicating that the fluorescein molecule generated in the macropores of the SiO_2 nanotubes can immediately diffuse out of the nanotube. This observation was used in the control experiment of the macropores in Figure 3E (in the main text).

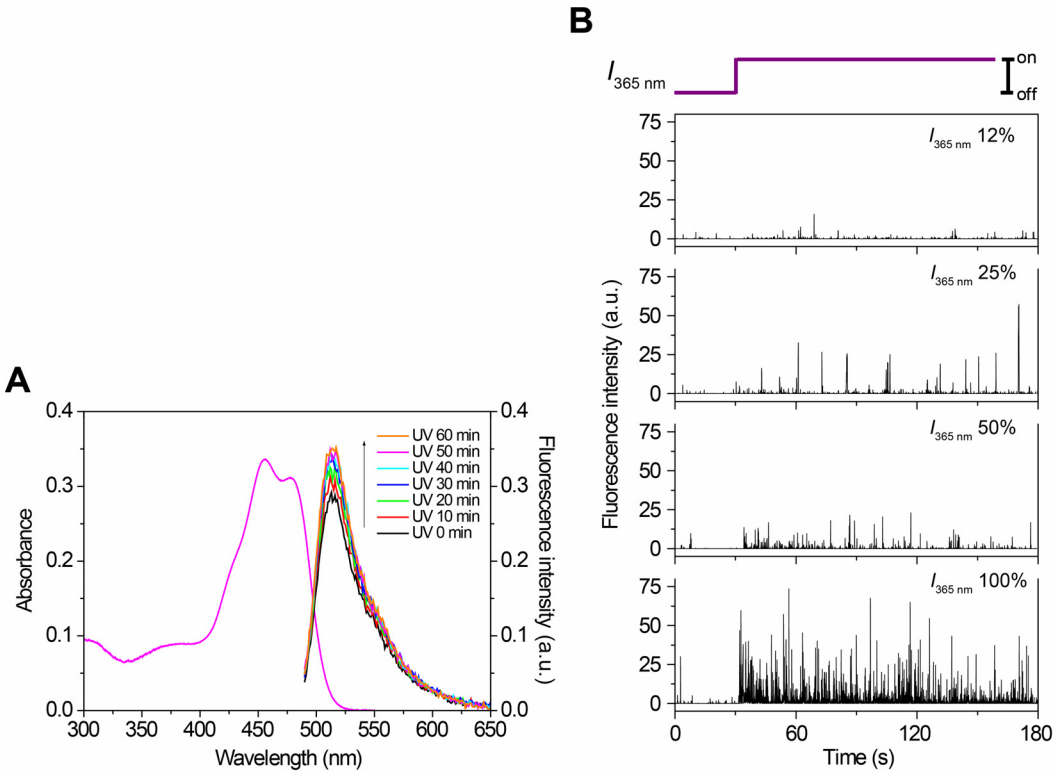

Figure S6. (A) Absorption spectra of 1.4×10^{-5} M APF phosphate buffer solution and the emission spectra of 500 nM APF phosphate buffer solution (pH 7.4) with dispersed TiO_2 nanotubes (0.5 mg ml^{-1}) during the 365-nm UV irradiation. The fluorescence intensity slightly increased due to the auto-oxidation. (B) Dependence of the UV irradiation power on the auto-oxidation of APF in a single SiO_2 nanotube immersed in the phosphate buffer solution of 500 nM APF (pH 7.4). The intensity of the UV light is weakened using the neutral density filter. By increasing the UV irradiation power, the frequency of the auto-oxidation of APF dramatically increased. In contrast, the auto-oxidation of APF is significantly suppressed during the weak UV irradiation.

References.

(1) Hoffmann, M. R.; Martin, S. T.; Choi, W.; Bahnemann, D. W. *Chem. Rev.* **1995**, *95*, 69–96.

(2) Nakamura, R.; Nakato, Y. *J. Am. Chem. Soc.* **2004**, *126*, 1290–1298.

(3) Kubo, W.; Tatsuma, T. *J. Am. Chem. Soc.* **2006**, *128*, 16034–16035.

(4) Murakami, Y.; Kenji, E.; Nosaka, A. Y.; Nosaka, Y. *J. Phys. Chem. B* **2006**, *110*, 16808–16811.

(5) Murakami, Y.; Endo, K.; Ohta, I.; Nosaka, A. Y.; Nosaka, Y. *J. Phys. Chem. C* **2007**, *111*, 11339–11346.

(6) Ishibashi, K.; Fujishima, A.; Watanabe, T.; Hashimoto, K. *J. Photochem. Photobiol. A* **2000**, *134*, 139–142.

(7) Nosaka, Y.; Komori, S.; Yawata, K.; Hirakawa, T.; Nosaka, A. Y. *Phys. Chem. Chem. Phys.* **2003**, *5*, 4731–4735.

(8) Naito, K.; Tachikawa, T.; Fujitsuka, M.; Majima, T. *J. Phys. Chem. C* **2008**, *112*, 1048–1059.

(9) Imai, H.; Takei, Y.; Shimizu, K.; Matsuda, M.; Hirashima, H. *J. Mater. Chem*. **1999**, *9*, 2971–2972.

(10) Kovtyukhova, N. I.; Mallouk, T. E.; Mayer, T. S. *Adv. Mater.* **2003**, *15*, 780–785.

(11) Gell, C.; Brockwell, D.; Smith, A. *Handbook of Single Molecule Fluorescence Spectroscopy*; Oxford University Press: New York, 2006.

(12) Sjöback, R.; Nygren, J.; Kubista, M. *Spectrochim. Acta. A* **1995**, *51*, L7–L21.

(13) Furlong, D. N.; Parfitt, G. D. *J. Colloid. Inter. Sci.* **1978**, *65*, 548–554.

(14) Franks, G. V. *J. Colloid. Inter. Sci.* **2002**, *249*, 44–51.

(15) Wu, H.-P.; Cheng, T.-L.; Tseng, W.-L. *Langmuir* **2007**, *23*, 7880–7885.

(16) Suomi, J.; Ylinen, T.; Håkansson, M.; Helin, M.; Jiang, Q.; Ala-Kleme, T.; Kulmala, S. *J. Electroanal.*

Chem. **2006**, *586*, 49–55.

(17) (a) Calculated from E_{CB} = –0.130 –0.059pH V vs NHE.[17b] (b) Duonghong, D.; Ramsden, J.; Grätzel, M. *J. Am. Chem. Soc.* **1982**, *104*, 2977–2985.

(18) Eigen, M.; Riglar, R. *Proc. Natl. Acad. Sci.* **1994**, *91*, 5740–5747.

(19) Lakowicz, J. R. *Principles of Fluorescence Spectroscopy*, 3rd ed.; Springer-Verlag, 2006.

(20) (a) Calculated from the equation of Brownian motion in one dimension, $\langle r^2 \rangle = 2Dt$, where $\langle r^2 \rangle$ is the mean-square displacement, D is the diffusion coefficient of fluorescein in solution (2.8×10^{-10} m^2 s^{-1}),[20b] and t is the time resolution (33 ms). (b) Chattopadhyay, K.; Saffarian, S.; Elson, E. L.; Frieden, C. *Proc. Nat. Acad. Sci. USA* **2002**, *99*, 14171–14176.